NARROWBAND PHOTORECEIVER FOR ANALOG RADIO-OVER-FIBER IN THE 24.25-29.5 GHZ BAND

Laurens Bogaert[1,2,], Haolin Li[1], Kasper Van Gasse[2], Joris Van Kerrebrouck[1], Johan Bauwelinck[1], Gunther Roelkens[2], and Guy Torfs[1]*

[1] *IDLab, INTEC, Ghent University - imec, 9052 Ghent, Belgium*
[2] *Photonics Research Group, INTEC, Ghent University - imec, 9052 Ghent, Belgium*
**Laurens.Bogaert@UGent.be*

Keywords: 5G MOBILE COMMUNICATION, MILLIMETER WAVE CIRCUITS, LOW-NOISE AMPLIFIERS, SILICON PHOTONICS, OPTOELECTRONIC DEVICES

Abstract

The presented narrowband photoreceiver, optimized for a 27.5-29.5 GHz Analog-RoF link, is based on a 3-stage GaAs narrowband low noise amplifier which offers 24.4-dB gain, 2.1-dB noise figure and 26.6-dBm OIP3. An rms-EVM of 2.46/3.47% is achieved for 100/400-MBaud 16-QAM over the 24.25-29.5 GHz band.

1. Introduction

The ever-increasing demand for high-speed wireless data connectivity will result in the need for the deployment of smaller communication cells [1]. To make such a densification of the network possible, centralized approaches are of paramount importance. Radio-over-Fiber (RoF) has been proposed as a possible architecture and is nowadays typically implemented digitally with the Common Public Radio Interface (CPRI). Analog Radio-over-Fiber (ARoF) on the other hand enables low-complexity, low-cost remote radio heads (RRH) that are required to make such a small cell communication network feasible [2] while offering improved spectral efficiencies compared to CPRI.

Communication using the ARoF principle starts from a continuous wave laser line which is modulated by an analog signal and transported over fiber. At the receiver, the optical signal needs to be converted back to the electrical domain. This requires high-speed photodetectors that are either co-integrated with a high-speed amplifier and antenna or directly connected to an antenna [3]. Typical implementations of the receiver use a broadband transimpedance amplifier (TIA) to boost the RF signal generated at the output of the photodetector. This requires the bandwidth of the TIA to exceed the carrier frequency of the narrowband signal.

However, wireless communication schemes are based on narrowband signals. Consequently, broadband amplification is typically suboptimal because of constraints imposed by the transimpedance limit [4]. In previous work, it was shown how resonant inductive peaking at the input of the TIA can boost the performance of conventional broadband transimpedance amplifiers for narrowband communication [5]. Similarly, dedicated narrowband photoreceivers [6-10] can be looked at to make optimal use of the narrowband nature of the future generation wireless bands. In such an approach, one can design the receiver to get an optimal power transfer from the photodetector to the load for a given frequency range instead of having suboptimal current-to-voltage conversion over a large band as is the case for broadband TIAs. In this work, we present a narrowband photoreceiver comprising a Ge-on-Si photodetector and a GaAs low noise amplifier (LNA). This photoreceiver has been designed and tested for communication in the 27.5 - 29.5 GHz band. During the link experiments, special attention was given to the extended spectrum of 24.25 - 29.5 GHz corresponding to 5G new radio interface specifications nr257 and nr258 [11].

2. Narrowband Photoreceiver

For the narrowband photoreceiver, a dedicated LNA was constructed starting from a readily available Ge photodetector (Fig. 1). On the silicon photonics IC, not only a Ge photodetector is present, but also a MZM is constructed to eventually allow for the design of an entire transceiver. The photodetector itself accounts for 220x160 µm and is therefore negligible in size compared to the rest of the assembly.

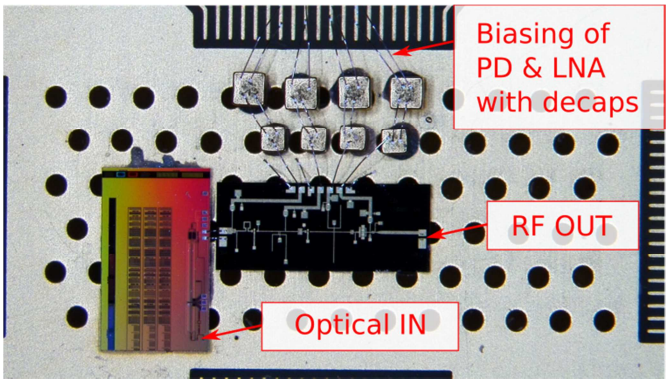

Fig. 1 Narrowband photoreceiver assembly

The input circuit for which the LNA was designed consists of a photodetector-wirebond combination (Fig. 2). The photodetector can be approximated as a parallel combination of a current source – generating a current proportional to the incident optical power – and a junction capacitance. Losses of the photodetector are modelled by adding a resistance in series with this parallel combination. The resistance is independent of the applied voltage ($R_s \approx 45\ \Omega$) while the

junction capacitance C_j decreases with increasing bias voltage. The photodetector capacitance for which the LNA was designed is 55 fF and this photodetector capacitance can be tuned between 71 and 47 fF by increasing the photodetector reverse bias between 0 and 3 V. This extra degree of freedom allows for compensation of the tolerances on the wirebond length. The nominal wirebond inductance L_{wb} that was adopted in the design is 495 pH. For the given values of the photodetector impedance and wirebond inductance, the source impedance results in 45-j12.89 Ω at 28.5 GHz. Starting from this source impedance the first stage of the LNA was designed by looking at an optimal trade-off between noise and gain matching while making sure that input and output return loss are well below -10 dB and that unconditional stability is ensured [12]. An internal bias tee is included in the input matching network of the LNA to make sure that the photodetector can be biased and that the DC current generated by the photodetector is not saturating the LNA. The design of the second and third stage mainly focuses on providing extra gain while impedance matching and unconditional stability are preserved. Additionally, the third stage uses a significantly larger HEMT transistor to provide sufficient linearity for the whole LNA.

The final implementation of the photoreceiver can be seen in Fig. 1 where the photodetector was implemented on imec`s silicon photonics platform iSiPP50G [13] while the LNA was designed in a 0.1 µm pHEMT GaAs technology [14]. For the constructed assembly, a hybrid integration approach was followed where the photodetector is wirebonded to the dedicated low noise amplifier (Fig. 2).

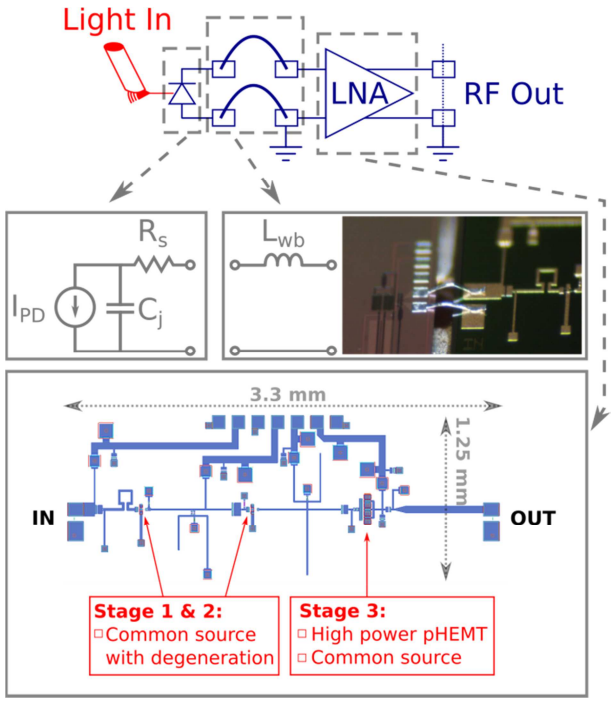

Fig. 2 Schematic overview of the photoreceiver

The three-stage LNA (Fig. 2) offers up to 24.4 dB small signal gain which results in a transimpedance of about 937 V/A or equivalently 750 V/W for the photoreceiver (responsivity of the photodiode ≈ 0.8 A/W). The LNA has a noise figure of 2.1 dB when fed from the Ge photodetector. This translates into an input-referred current noise of approximately 10.7 pA/√Hz. Additionally, input and output return losses below -12 dB are obtained over the 27.5 to 29.5 GHz band. For this paper, the LNA supply was chosen to be 3 V, resulting in a power consumption of 303 mW and an output referred third order intercept point (OIP3) of 26.6 dBm. In case of a 2 V supply the power consumption reduces to 160 mW at the cost of linearity degradation (OIP3 = 22.2 dBm). While the LNA was initially designed for optimal performance in the 27.5 - 29.5 GHz band, it is useful to explore the device performance in other frequency bands including the 24.25 - 29.5 GHz band specified in 5G new radio standards nr257 and nr258. This extended band can be covered with a small signal gain of at least 21.9 dB and a noise figure below 3.06 dB but with increased reflections. Input and output matching drop to respectively -6.3 dB and -5.5 dB around 24.25 GHz.

3. Frequency Dependent Behaviour

To characterize the opto-electronic small signal transmission behaviour (S_{21}) of the narrowband photoreceiver, a 40 Gbps LiNbO3 Mach-Zehnder modulator (MZM) was used at the transmitter (*Fujitsu FTM7937EZ*). The frequency response of the transmitter was also characterized using a 50 GHz photodetector *XPDV21x0RA* from *Finisar* and de-embedded from the measured S_{21}. The resulting calibrated transmission characteristic is shown in Fig. 3.

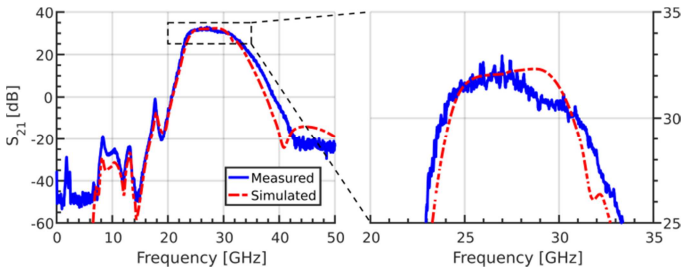

Fig. 3 S_{21} of photoreceiver after calibration of transmitter

Besides, the simulated transmission behaviour is also visualized in Fig. 3 with the dashed line and shows good agreement with measurements. The measured 3-dB cut-off frequencies are situated around 23.5 GHz and 31.5 GHz.

4. Radio-over-Fiber Link Setup

The photoreceiver has been tested as part of the ARoF link depicted in Fig. 4. The transmitter consists of a continuous wave laser, polarization controller (PC), Mach Zehnder modulator, Erbium doped fiber amplifier (EDFA) and variable optical attenuator (VOA). The laser emits 13 dBm 1550 nm continuous wave light. Subsequently, the light is modulated by the previously introduced MZM biased at its quadrature point. The RF signal fed to the modulator is constructed by first generating in-phase (I) and quadrature (Q) signals with an arbitrary waveform generator (AWG, *Keysight M8195A*) at an IF frequency of 2.5 GHz. Subsequently, an I/Q-mixer (*Hittite HMC-1063*) is used to implement the up-conversion to the correct RF frequency. The local oscillator (LO) frequency can be tuned to change the RF frequency of the signal driving the MZM. This

transmission scheme results in a modulation index of around 0.15. The last part of the transmitter is an EDFA-VOA combination which allows tuning of the optical power fed to the ARoF link.

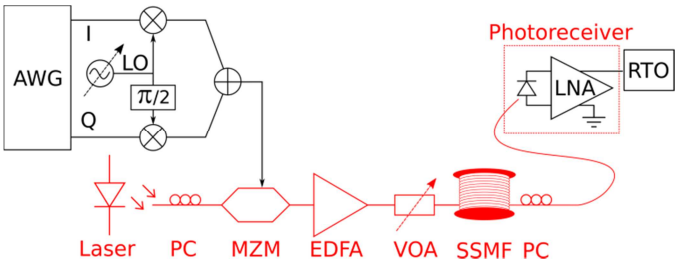

Fig. 4 Setup used for ARoF experiments

After the modulation and power tuning of the optical output of the transmitter, the signal is then transported over standard single mode fiber (SSMF) before reaching the receiver. At the receiver, the polarization of the incoming light is optimized and afterwards the signal is fed to the photoreceiver. Coupling from fiber to chip is realized by using a grating coupler which will result in about 5 dB insertion loss. The adopted LNA supply is 3 V while the photodetector uses 1 V reverse biasing. The output of the photoreceiver is then monitored by a real-time oscilloscope (RTO, *Keysight DSA-Z 634A*).

5. Radio-over-Fiber Link Results

The 5G new radio standards nr257 and nr258 target channel bandwidths of 50, 100, 200 and 400 MHz [11]. The ARoF link depicted in Fig. 4 is evaluated with 100 and 400 MBaud 16-QAM signals (roll-off factor of 0.28).

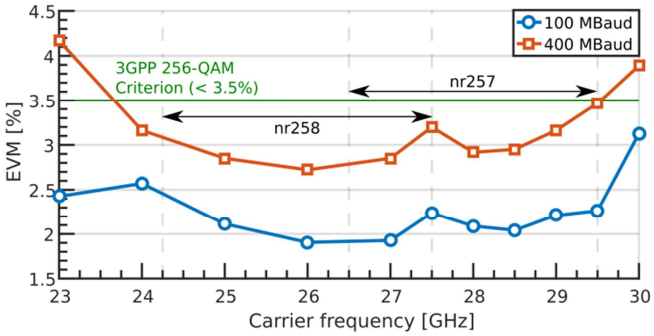

Fig. 5 rms-EVM as a function of the carrier frequency

The first experiment consists of sweeping the carrier frequency from 23 to 30 GHz. After acquisition by the RTO, 9-tap equalization was used to compensate bandwidth limitations in the probing setup and the MZM transmission characteristic. Fig. 5 shows the influence of the changing baudrate and carrier frequency on the root-mean-square (rms) value of the error vector magnitude (EVM) in the absence of SSMF (optical back to back, OB2B) with approximately 0 dBm on-chip optical power incident on the photodetector (resulting in approximately -8 dBm RF power at the output of the photoreceiver). The adopted EVM definition normalizes relative to the average power. These measurements show that the photoreceiver can be used for the nr257 and nr258 standards while offering an rms-EVM below 2.46 and 3.47 % for respectively 100 MBaud and 400 MBaud channels. These values satisfy 3GPP requirements for 16-QAM (< 12.5 %), 64-QAM (< 8 %) and 256-QAM (< 3.5 %) [15].

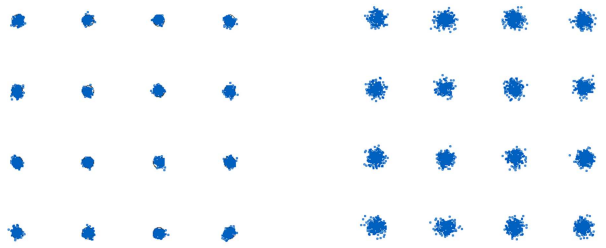

(a) **(b)**

Fig. 6 Constellation diagram at the RTO when transmitting (a) 100 MBaud, (b) 400 MBaud at 28 GHz over 21 km SSMF

Finally, link experiments with 21 km SSMF were performed at a 28 GHz carrier frequency. The power incident on the photodetector in this configuration is -4 dBm. The constellation diagram measured at the RTO for a 100 and 400 MBaud signal are displayed respectively in Fig. 6(a) and Fig. 6(b). The corresponding rms-EVM values are respectively 2.88 and 5.56 %.

6. Conclusion

In this paper, the design of an integrated narrowband photoreceiver for an ARoF link is presented and demonstrated. The photoreceiver retrieves the RF signal back from the optical carrier at a Ge photodetector and subsequently boosts the bandpass signal with a GaAs LNA. Adopting a narrowband LNA design methodology rather than a broadband TIA design for the photoreceiver allows for a more optimal trade-off between the minimization of the noise and maximization of the gain. The main reason for this is that the LNA is designed for optimal operation within a limited band while a broadband TIA requires optimization from DC up to the RF frequency resulting in suboptimal performance in the frequency range of interest.

The presented LNA offers a gain of 24.4 dB, introduces a noise figure of only 2.1 dB and has an OIP3 of up to 26.6 dBm. The 3-dB cut-off frequencies for this photoreceiver are found at 23.5 GHz and 31.5 GHz. ARoF link experiments with this device show coverage of the nr257 (26.5 - 29.5 GHz) and nr258 (24.25 - 27.5 GHz) bands with rms-EVM values below 2.46 and 3.47 % for 100 and 400 MBaud 16-QAM communication respectively.

7. Acknowledgements

This work was supported by the Ghent University Special Research Fund (BOF14/GOA/034), the Methusalem funding of the Flemish government, the Air Force Office of Scientific Research (AFOSR) (FA95501810015), the European Research Council Grant ATTO (695495), and by the H2020 5GPPP Phase II project 5G-PHOS (761989).

8. References

[1] Andrews, J. G., Buzzi, S., Choi, W., et al.: 'What Will 5G Be? ', IEEE J. Sel. Areas Comm., 2014, **32**, (6), pp. 1065–1082, DOI: 10.1109/JSAC.2014.2328098

[2] Kawanishi, T., Kanno, A., Freire, H. S. C.: 'Wired and Wireless Links to Bridge Networks', IEEE Microw. Mag., 2018, **19**, (3), pp. 102–111, DOI: 10.1109/MMM.2018.2801638

[3] Torfs, G., Li, H., Agneessens, S., et al.: 'ATTO: Wireless Networking at Fiber Speed', J. Lightwave Technol., 2018, **36**, (8), pp. 1468–1477, DOI: 10.1109/JLT.2017.2783038

[4] Sackinger, E.: 'The Transimpedance Limit', IEEE Trans. Circuits Syst. I, Reg. Papers, 2010, **57**, (8), pp. 1848-1856, DOI: 10.1109/TCSI.2009.2037847

[5] Bogaert, L., Van Kerrebrouck, J., Abbasi, A., et al.: 'Resonant Optical Receiver Design by Series Inductive Peaking for Sub-6 GHz RoF', Wiley Microw. Opt. Technol. Lett., 2017, **59**, (9), pp. 2279–2284, DOI: 10.1002/MOP.30721

[6] Miras, A., Legros, E., Vuye, S., et al.: '40 GHz-Narrowband Photoreceiver for Clock Recovery in 40 Gbit/s Optical Transmission Systems', IEEE MTT-S Digest, Denver, United States of America, June 1997, pp. 1709–1712, DOI: 10.1109/MWSYM.1997.596769

[7] Umbach, A., Engel, T., Bach, H.-G., et al: 'Technology of InP-Based 1.55-µm Ultrafast OEMMIC`s: 40-GBit/s Broad-Band and 38/60-GHz Narrow-Band Photoreceivers', IEEE J. Quantum Electron., 1999, **35**, (7), pp. 1024–1031, DOI: 10.1109/3.772171

[8] Leven, A., Hurm, V., Reuter, R., Rosenzweig, J.: 'Design of Narrow-Band Photoreceivers by means of the Photodiode Intrinsic Conductance', IEEE Trans. Microw. Theory Tech., 2001, **49**, (9), pp. 1908–1913, DOI: 10.1109/22.954806

[9] Umezawa, T., Kashima, K., Kanno, A., et al.: '100-GHz Fiber-Fed Optical-to-Radio Converter for Radio- and Power-Over-Fiber Transmission', IEEE J. Sel. Topics Quantum Electron., 2017, **23**, (3), DOI: 10.1109/JSTQE.2016.2611638

[10] Fedderwitz, S., Leonhardt, C. C., Honecker, J., et al.: 'A high linear and high power photoreceiver suitable for analog applications', IEEE Photonics Conference 2012, Burlingame, United States of America, September 2012, DOI: 10.1109/IPCon.2012.6358615

[11] 3GPP, 'TR 38.815: New Frequency Range for NR (24.25-29.5 GHz) – Release 15', 2018

[12] Henkes, D. D.: 'A Design Tool for Improving the Input Match of Low Noise Amplifiers', High Frequency Electronics, 2007, **6**, (2), pp. 54–64

[13] Pantouvaki, M., Srinivasan, S. A., Ban, Y., et al.: 'Active Components for 50 GB/s NRZ-OOK Optical Interconnects in a Silicon Photonics Platform', J. Lightwave Technol., 2017, **35**, (4), pp. 631–638, DOI: 10.1109/JLT.2016.2604839

[14] Teyssandier, C., Stieglauer, H., Byk, E., et al.: '0.1µm GaAs pHEMT Technology and Associated Modelling for Millimeter wave Low Noise Amplifiers', Proc. EuMIC, Amsterdam, Netherlands, October 2012, pp 171–174

[15] 3GPP, 'TS 36.104: LTE; Evolved Universal Terrestrial Radio Access (E-UTRA); Base Station (BS) radio transmission and reception – Release 15, v. 15.3.0', 2018